
The Application of Fault Simulation to Machine Diagnostics and Prognostics

Robert B. Randall

*School of Mechanical and Manufacturing Engineering,
University of New South Wales, Sydney 2052, Australia*

(Received 5 May 2009; accepted 11 May 2009)

The early development of machine diagnostics and condition monitoring was based on measurements from actual failures, but these cannot be predicted or arranged to occur when and where desired. In recent years it has become possible to make simulation models of a machine, such as a gearbox or engine, including the simulation of various faults of different types, severity, and location. There are a number of benefits from doing this, the first being to be able to produce sufficient representative signals to train automated fault recognition algorithms, such as artificial neural networks, as it is not economically viable to experience the number of actual failures required. Being able to produce signals from faults of different sizes and locations can be useful in the development of diagnostic and prognostic procedures — the latter, for example, by being able to develop appropriate trend parameters. Finally, the effects of faults in complex machines are often based on nonlinear interactions, which are difficult to foresee, and the simulation modelling of the whole machine can be very useful to obtain a physical understanding of these complex interactions. This paper illustrates these principles using examples of rolling element bearings, gears, geared systems (including bearings), and internal combustion engines, with favourable results in all aspects.

1. INTRODUCTION

There are three main areas where fault simulation is valuable in machine diagnostics. The first has to do with the training of artificial neural networks (ANN) and similar classifiers to perform diagnostics and prognostics of faults in machines. Many authors have proposed using ANN to perform automated machine diagnostics, by learning the features that characterize various types of faults. However, neural networks must be trained using a considerable amount of data to characterize each condition to be detected and classified, with a certain amount of random variation typical of the variations in operating conditions experienced by a machine in a given condition. Virtually, the only condition which would provide sufficient data to achieve this goal is the normal condition, and, so, ANN can be used to detect this, as well as departures from it. On the other hand, it would not be economical to actually experience the number of faults and failures of each type required to train ANN for all fault conditions.

Moreover, real faults cannot be made to appear at will; one usually has to wait until they occur, which may be very infrequent. Another problem with some of the papers that describe the use of ANN for diagnostics is that the data on which they are trained comes from a particular machine (often a laboratory test machine with seeded faults). Though the training process may be successful in this situation, it is not at all clear how the results could be extended to even a very similar machine, let alone the wide range of machines in operation, where it is impossible to experience the full gamut of faults for which the machine must be protected.

Therefore, the only way to viably use ANN for machine diagnostics and prognostics is to use simulated signals to train them. The level of sophistication of the simulation required depends on the application, but this paper describes a range of applications with different levels of sophistication. In general, it is desirable for the simulations to cover as wide a range of

situations as possible, but there are cases with very valuable machines (e.g., turbogenerator sets) where it is worth making a detailed simulation model specific to a particular machine, (e.g.,^{1,2}).

Simulation models can also be used to provide signals to test new diagnostic methods and to compare different methods, rather than being forced to rely on randomly captured case histories, or data generated by laboratory test rigs, — often with seeded faults.

A final application of simulation of machine faults is to give a better understanding of signal characteristics that have been experienced in practice, where, for example, nonlinearities can give interactions which are difficult to predict, and this can be used to help explain anomalies.

This paper illustrates a number of these applications, using as examples the simulation of rolling element bearings, gears, and geared systems, as well as the interactions between gears and bearings. The simulation of signals from reciprocating machines (such as diesel and spark ignition engines) is also covered, mainly by simulation of their torsional vibrations, but a project is also underway to simulate cylinder head and block vibrations.

The examples that are illustrated are of increasing complexity. As an example, local faults in rolling element bearings give very distinctive patterns in the spectra of envelope signals obtained by demodulating frequency bands dominated by the faults,³ and such spectra can be simulated directly, without having to go via the time signals. This type of modelling, while general, would only indicate whether a particular type of fault were present, and it would be difficult for it to indicate degree of severity, although this is a goal of future development. The type of simulation ranges in complexity up to the modelling of a particular machine, showing how the small amount of actual measurement data available (for good and faulty condition) can be used to update and calibrate the model, and give confidence

in its predictions for non-experienced cases.

In the following, the cases of rolling element bearings, gears and geared systems (including the incorporation of detailed bearing models), and reciprocating machines such as spark ignition and diesel engines, are treated separately.

2. ROLLING ELEMENT BEARINGS

Figure 1 illustrates typical signals produced by local faults in rolling element bearings, for the case of a constant unidirectional load (vertically down in this case). Each basic type of fault, in the outer race, inner race or rolling element produces very characteristic patterns in the time signals, and, in particular, in the “envelope signals” obtained by amplitude demodulation of the time signals. An outer-race fault, for example, would always be in the load zone, and in principle give a uniform series of impulse responses (with repetition frequency BPFO) as the successive rolling elements strike the fault. An inner-race fault, on the other hand, passes through the load zone at shaft speed, so the series of impulse responses at BPFi are modulated by the shaft speed (additionally because the signal transmission path is also varying at this rate). Similarly, a fault on a rolling element passes through the load zone at cage speed, so the series of (pairs of) pulses at BSF is modulated by this frequency.³ In Reference⁴ it is shown that spectrum analysis gives very little diagnostic information about the repetition rates of the faults (or their modulations), because of small random fluctuations of the pulse period, but frequency analysis of the envelope (and even more so, the squared envelope) of the signals does reveal harmonics of the ballpass frequencies, as well as sidebands (and low harmonics) spaced at the modulating frequencies.

The characteristic fault frequencies on the signals depicted in Fig. 1 are given by the following equations:

$$BPFO = \frac{n f_r}{2} \left\{ 1 - \frac{d}{D} \cos \varphi \right\} \quad (1)$$

$$BPFi = \frac{n f_r}{2} \left\{ 1 + \frac{d}{D} \cos \varphi \right\} \quad (2)$$

$$FTF = \frac{f_r}{2} \left\{ 1 - \frac{d}{D} \cos \varphi \right\} \quad (3)$$

$$BSF = \frac{f_r D}{2d} \left\{ 1 - \left(\frac{d}{D} \cos \varphi \right)^2 \right\} \quad (4)$$

where n = no. of balls (rollers), f_r = shaft speed, d = ball (roller) diameter, D = pitch diameter and φ = load angle from radial.

These very distinctive patterns in the envelope spectra can be used to train ANN, at least for the simple go/no-go decision of whether the fault in question is present. In Reference⁵ feature vectors as described in Fig. 2, were extracted from envelope spectra corresponding to faults in bearings on a small test rig. Feature vectors are arrays of features characterising a particular condition, and used to train an ANN. The feature vectors are unscaled, and particular features must be related to typical values. In this case, spectrum peak values were sought in a range within 2% of the calculated frequencies of the fault, to allow for the normal slip (for inner-race faults, only BPFi has this uncertainty; sidebands are spaced at exactly shaft speed). Since an expert judges discrete envelope spectrum components

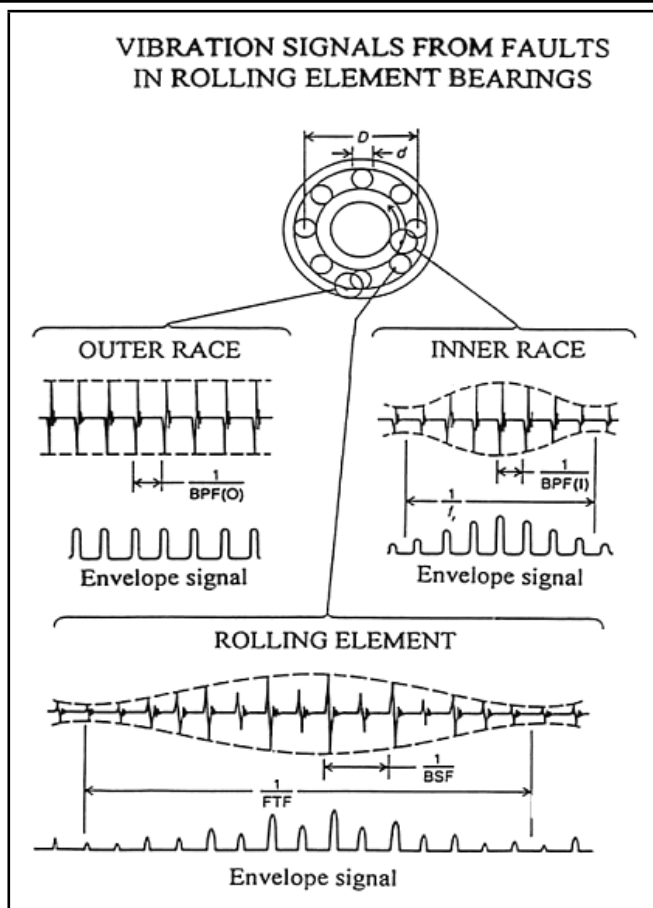


Figure 1: Typical signals and envelope signals from local faults in rolling element bearings: BPFO = ballpass frequency, outer race; BPFi = ballpass frequency, inner race; BSF = ball (roller) spin frequency; FTF = fundamental train frequency (cage frequency).

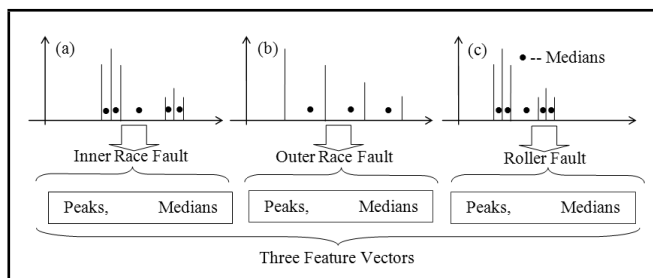


Figure 2: Feature vector construction — each pattern as an individual vector.

in comparison with the noise level in the spectrum, the median values were used as a reference level for this noise (since they are little affected by the appearance of a number of discrete peaks). Initially they were placed in the order in which they occur, but it was then realised that the order of the vector elements is irrelevant, so the median values were placed at the end of the array. Separate networks were trained for each type of fault, even when some bearings had more than one type of fault present.

Figure 3 on the left shows the resulting feature vectors for an inner-race fault, made up from some cases with inner-race fault only, and some with both inner and outer race faults. Moreover, both the “no-fault” and “outer race” data were used to train the “not inner race” classification. On the right are

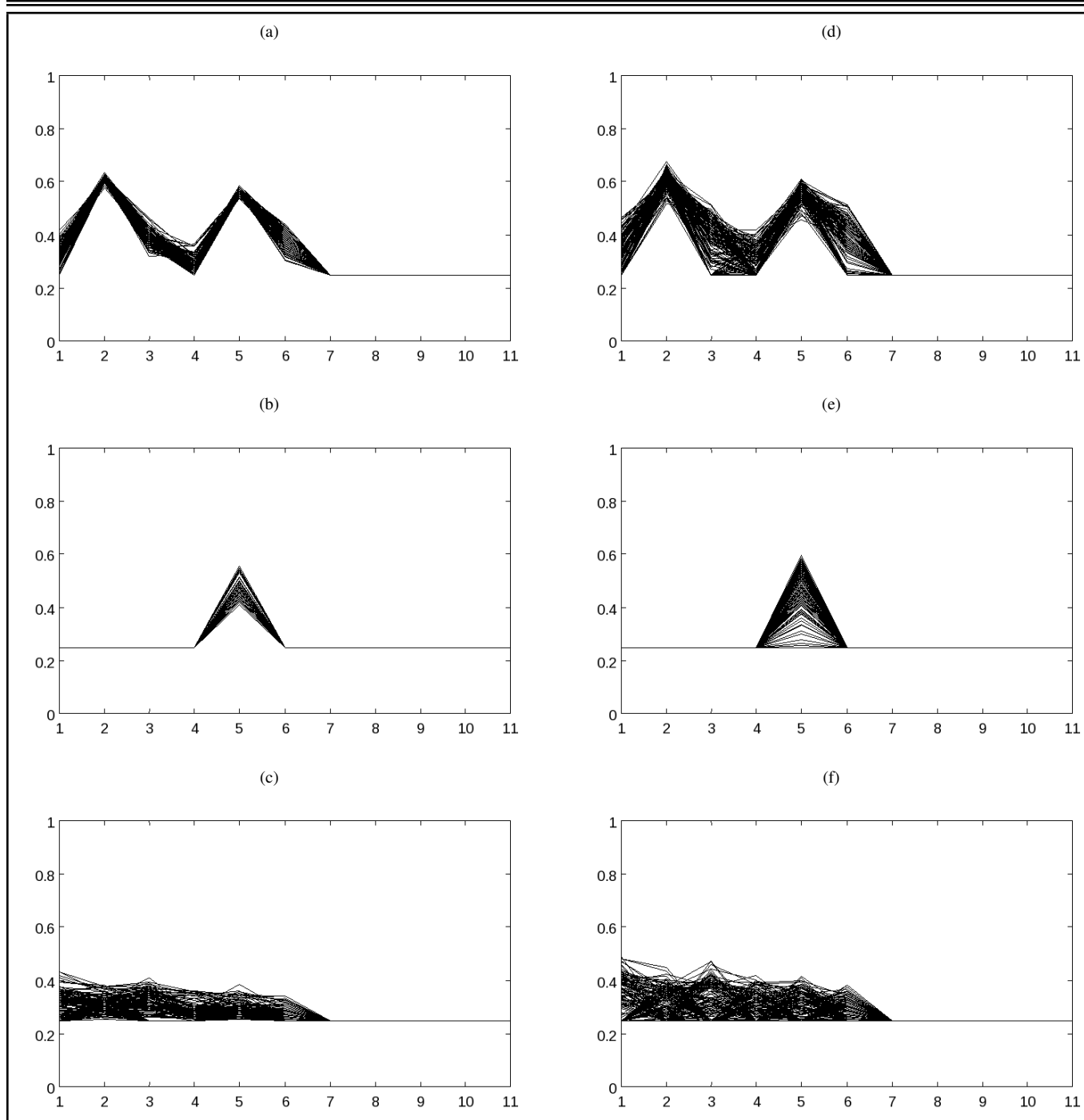


Figure 3: Feature vectors for inner-race fault frequencies: (a, d) inner race fault, (b, e) outer race fault, (c, f) no fault, (a, b, c) measured data, (d, e, f) simulated data.

shown feature vectors with the same mean values, but a three times greater standard deviation, which were successfully used to train networks intended to be more generally applicable to inner-race faults in general. When tested on data from a wide range of case histories from machines of different sizes and speeds (eight cases), they were found to have a 100% success rate in determining whether the bearing in question had the fault or not, though it would not have been possible to determine the degree of severity of the fault. This is, thus, the simplest form of simulation, based on an expansion of actual measured data to simulate the general case. It cannot, of course, be used to generate data to test diagnostic algorithms. The application of the method is dependent on being able to extract the bearing signal from background noise and masking by other

vibration signals, but a very powerful procedure for achieving this has been presented in Reference.⁶

A more detailed simulation of faults in rolling element bearings was presented in Reference.⁷ It is for a specified bearing geometry, including the amount of clearance or preloading of the bearing, which has a big effect on the size of the load zone, and whether individual rolling elements become unloaded. Shaft orbits can become chaotic, although always bounded. It is based on a two-dimensional bearing model presented by Fukata et al. in Reference⁸ but includes the random slip actually encountered in bearing signals.

A similar bearing model has since been incorporated into a gearbox simulation model, which is described in a separate section below and will be discussed after that.

3. GEARS

Much work has been done over the years in simulating gear vibrations, but usually with a view to noise and vibration reduction. Simulation of gear faults is somewhat more limited. Reference⁹ included simulations by Vexel and Cahouet of spalls, and were used along with actual measured data to test a new diagnostic method proposed by the other authors. Ref. [10] simulated the effects of a tooth-root crack on gear vibrations and included the effects of friction, which is often otherwise ignored. Reference¹¹ also simulated faults in a gear dynamic model, but more by statistical variations of transmission error parameters.

Reference¹² proposed a method of simulating meshing gears with two types of faults: a tooth-root crack (TRC) and a spall, since these have similar symptoms according to classical detection and diagnostic methods, but would have very different prognoses. A finite element program (Marc) was first used to simulate the variation in transmission error for the two fault types under static conditions. Transmission error (TE) is the deviation in motion of the driven gear relative to the rotational motion of the driving gear for perfect conjugate action (constant output speed for constant input speed). It is synonymous with "motion error" (ME), which forms part of RME in Fig. 4. RME (relative motion error) is the difference in motion error caused by the introduction of the fault. As shown in Fig. 4(a), it was found that the TRC primarily gave a change in stiffness at the mesh when the faulty tooth was in mesh, and, thus, the change in TE was proportional to the load (as well as the size of crack), but for spur gears at least, the timing did not change because it always corresponded to the time of engagement of the faulty tooth (either with a single tooth pair or a double tooth pair); with the spall, however, (Fig. 3(b)), the main effect was geometric, due to the loss of metal, and was thus virtually independent of load. On the other hand, the length of the effect on the TE (in terms of roll angle) was proportional to the length of the spall in that direction.

These static models were then inserted into a lumped parameter dynamic model of the simulated gearbox to obtain typical dynamic TE and acceleration responses under a range of speed and load conditions. Figure 5(a) shows the actual test rig, and Fig. 5(b) shows the lumped parameter model (LPM) used to obtain dynamic responses. Figure 6(a) gives a comparison of the predicted TE for a tooth-root crack, and Fig. 6(b) gives a corresponding measured TE. Note that the shafts of the test rig are unusually long and slender, making them very flexible. This was originally done to place a shaft resonance in a frequency range where it could be excited by the toothmeshing frequency in the normal shaft speed range up to 12 Hz. However, it meant that the shaft flexibility is two orders of magnitude greater than that of the toothmesh (not modelled in the original FE model of the gears) and makes it difficult to detect the changes in stiffness given by the tooth-root crack. For this reason, nylon gears with a value of Young's modulus two orders of magnitude less than steel were used for the experimental validation of the simulation model in this figure.

Figure 6 shows that the simulation closely represents the measured characteristic of a tooth-root crack, and the measured TEs in Figs. 7 and 8 agree with the predictions of the simulation model with respect to the effects of load on the cases with tooth-root crack and spall, respectively. Basically, the devia-

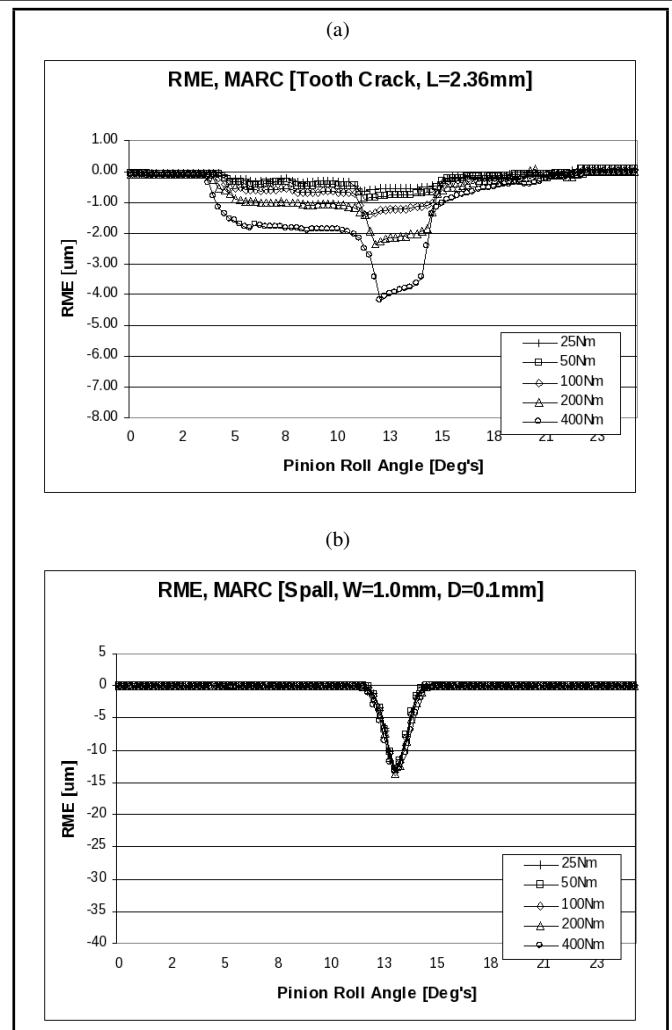


Figure 4: The TEs of gears with (a) a tooth crack and (b) a spall, for different loads.

tions in TE are proportional to the load (as is the toothmesh component) for the crack, but do not change with load for the spall. Simulated signals were used in Reference¹² to develop a differential diagnostic method to distinguish between cracks and spalls, and the results were largely borne out by the experimental measurements made by Endo as part of his PhD thesis (of which Figs. 6, 7 and 8 are examples).¹³ Many of the results of Endo's thesis have recently been published in Reference.¹⁴

It should be noted that in a recent paper by Mark and Reagor, it was pointed out that with naturally generated cracks (rather than the machined slots often used to simulate them), plastic deformation at the crack tip gives a permanent tooth deformation in addition to the elastic load dependent component, but this could be incorporated into the simulation.¹⁵

4. GEAR/BEARING SYSTEMS

The lumped parameter model of the gearbox in Fig. 5 was extended to include a bearing model similar to that in Reference.⁷ The form of the model is quite similar for the bearings and gears, with a time (or rotational angle) varying non-linear stiffness. Results for local faults have been published in Reference¹⁶ and for extended faults in Reference.¹⁷ In the so-called lumped parameter model (LPM) of the gearbox, the gears and shafts were modeled in some detail for both tor-

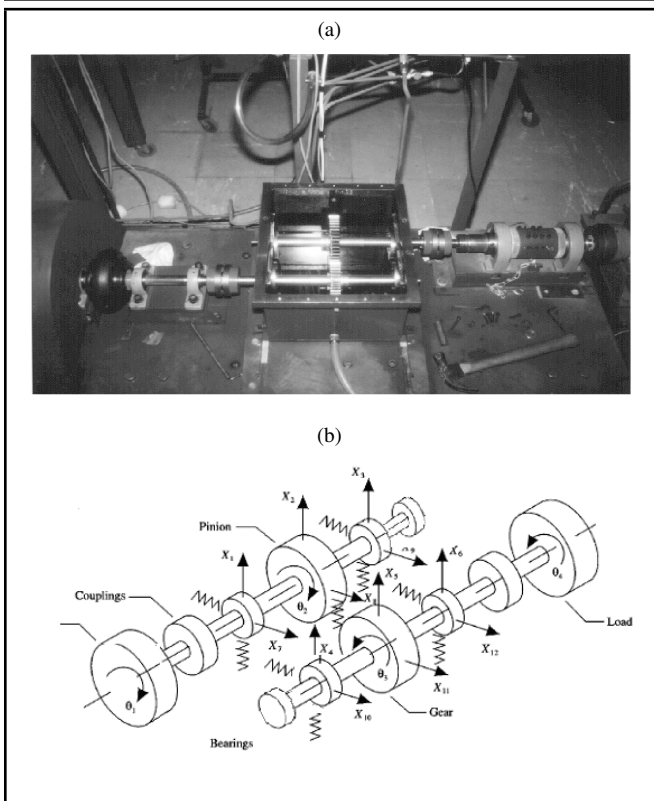


Figure 5: (a) The spur gear test rig. (b) Lumped parameter model.

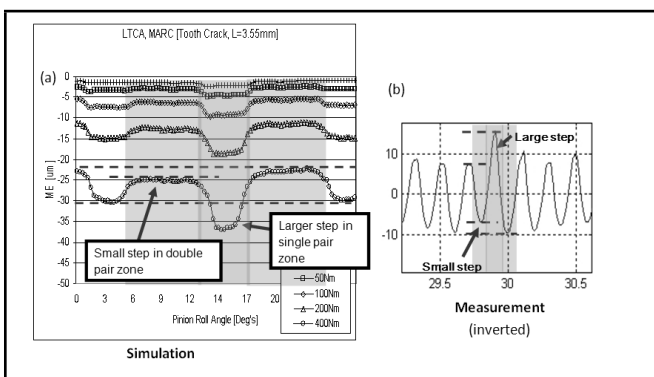


Figure 6: Comparison of simulated vs. measured TE for a tooth root crack.

sional and lateral deflections, but only a primitive model of

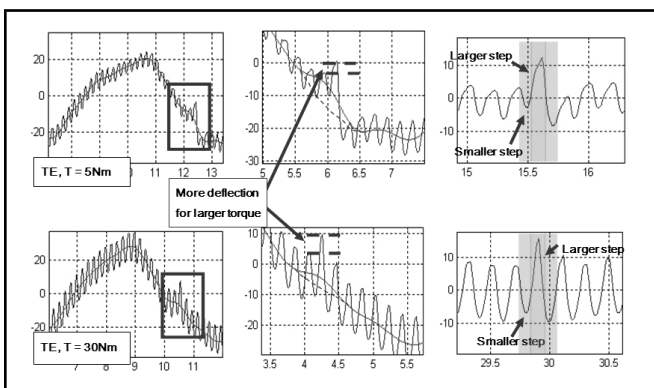


Figure 7: Variation of measured TE with load for a tooth-root crack.

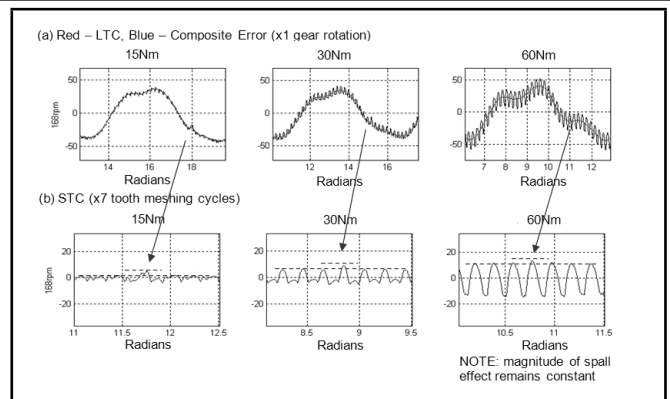


Figure 8: Variation of measured TE with load for a spall.

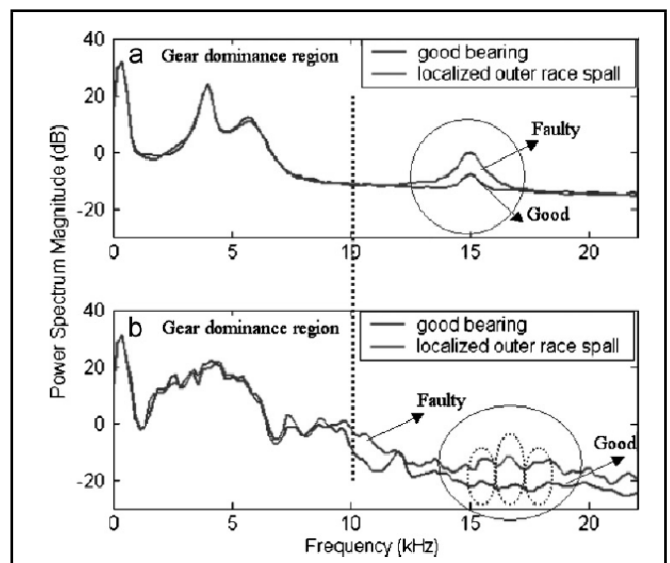


Figure 9: Comparison of autospectra for simulated and experimental localized outer-race fault.

the casing was made, with a low-frequency rigid body mode and a high-frequency (15 kHz) resonance typical of those demodulated to diagnose bearing faults.⁴ Figure 9 compares autospectra for the simulated and experimentally measured cases for a localized outer-race fault. Despite the considerable differences in the spectra (caused by the primitive casing model), Fig. 10 shows that bandpass-filtered signals and (squared) envelope spectra demodulated around the dominant high-frequency resonance were very similar. Similarly good results were achieved for localized inner-race and rolling-element faults.

The results for extended faults in Reference¹⁷ were reasonable but not so good. This could be ascribed to the fact that, as explained in Reference,¹⁸ extended bearing faults in gearboxes manifest themselves largely by modulating the gearmesh signals, because the gears are supported by the bearings. This modulation occurs over a wide frequency range, and is affected by the discrepancy in the response spectra in the “gear-dominance region,” as depicted in Fig. 9.

In a first attempt to correct this, a finite element (FE) model of the gearbox casing was made. A preliminary assumption was that the bearing blocks were so rigid that the dynamics of the thinner casing plates would have minimal effect on the forces at the bearings. The forces generated at the bearings by the LPM were thus applied to the modal model of the cas-

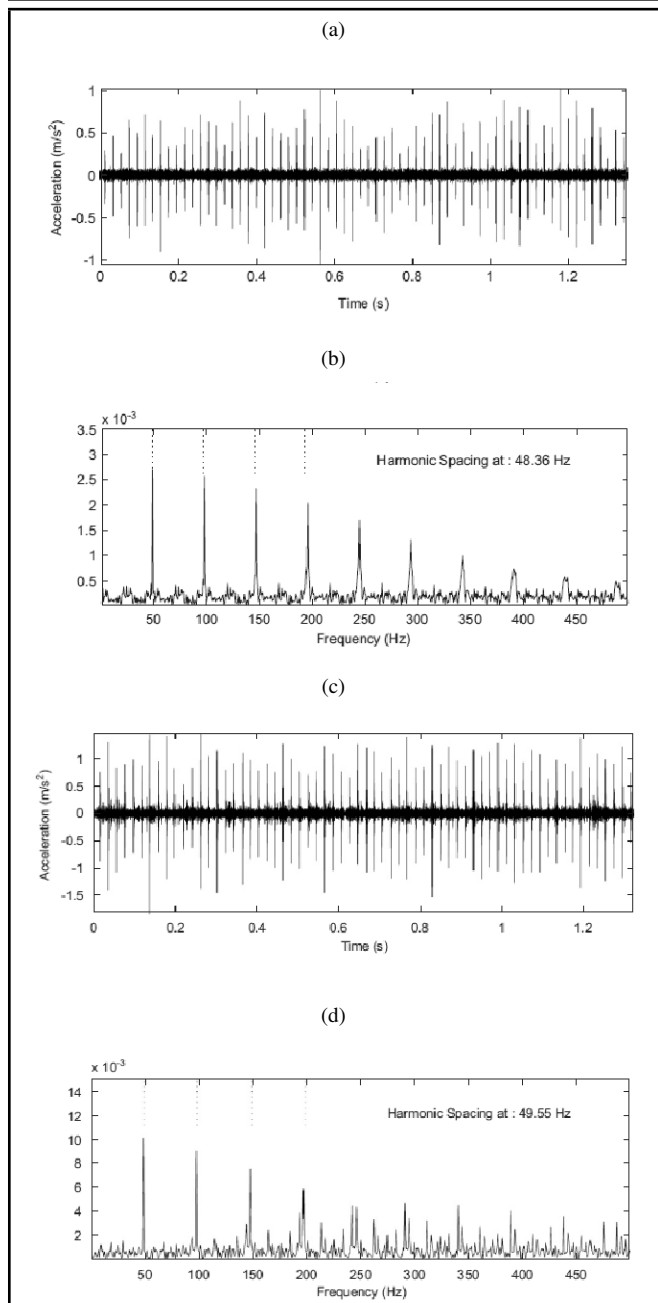


Figure 10: Time signals and squared envelope spectra for simulated and measured outer-race faults, bandpass filtered and demodulated around a high-frequency resonance: (a,b) simulated signal, (b,c) measured signal, (a,c) time signals, (b,d) envelope spectra.

ing from the FE model (updated to agree with experimental modal measurements for the modes up to about 1 kHz). The FE model was thus used to generate FRFs and impulse responses from the bearings to the measurement point, and the total response there simulated as a time signal by summing the convolutions of each bearing force with the corresponding impulse response.¹⁹ Figure 11 presents results from Reference¹⁹ comparing the spectral correlation functions for the two cases of simulation (original LPM and combination with the FE model) and an experimental measurement. In Ref. [18], it was shown that where the bearing fault interacts multiplicatively with the gearmeshing signal, as with an extended fault, the bearing frequencies can best be illustrated by the spec-

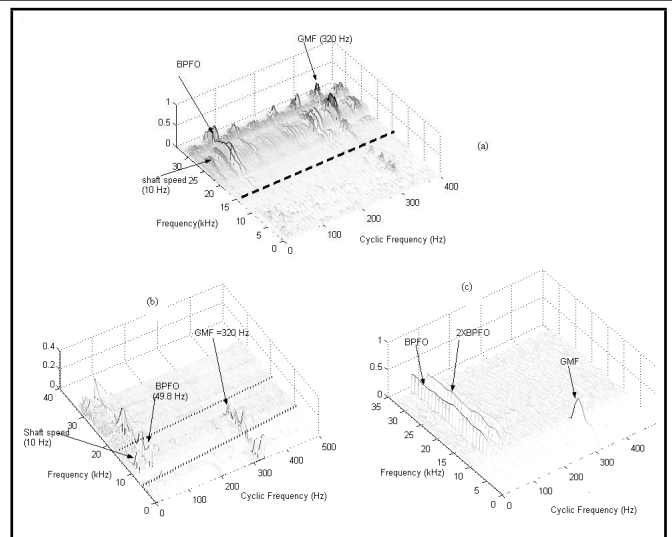


Figure 11: Spectral correlation function after removal of discrete-frequency components: (a) experimental, (b) combined model, (c) LPM model.

tral correlation function, which on one axis shows normal frequency (the resonances excited by the fault and noise modulation sidebands around the gearmesh harmonics) and on the other axis shows the “cyclic frequency” with which the modulation occurs. If discrete frequencies are first removed (e.g. the modulating effects from normal or faulty gear operation), the remaining signal can only come from bearing faults. Reference¹⁸ describes the case for an extended inner-race fault, but here we see that an extended outer-race fault also shows up at the BPFO (and as random modulation of the gearmesh frequency). The combined model is much closer to the measured result than the LPM result (and autospectra over the whole frequency range are much closer than in Fig.9), but the interaction between gears and bearings is still not fully represented.

An attempt is now being made to include the casing dynamics in the actual time-domain simulation, by including a reduced modal model from the FE model in that simulation. Results will be reported when they are available.

Before leaving the topic of gear/bearing systems, an anomaly will be shown that was responsible for us recognizing the two mechanisms by which bearing faults manifest themselves in gearboxes. It was reported in Reference.²⁰ Envelope spectra demodulated over four frequency bands gave anomalous results for an outer-race fault. When demodulated over the bands 6-24 kHz and 4-24 kHz, the BPFO and its harmonics were clearly shown. However, when demodulated over the intermediate band 5-24 kHz, the BPFO component disappeared. Demodulating the narrow band 5-5.5 kHz solved the mystery, as this included modulation sidebands around the fourth harmonic of gearmesh frequency. It was found that this component from modulation (Fig. 12(d)) had the same amplitude as the component from additive impulses at high frequency (Fig. 12(a)), but had opposite phase, so they the two cancelled each other, as shown in Fig. 12(b). Stronger modulation around the third harmonic of gearmesh frequency dominated in Fig. 12(c).

The question arises as to why the third and fourth harmonics of toothmesh frequency were modulated by the bearing fault, but not the first, second, or fifth. Similar patterns have been seen in some of our simulations of the UNSW gearbox test rig,

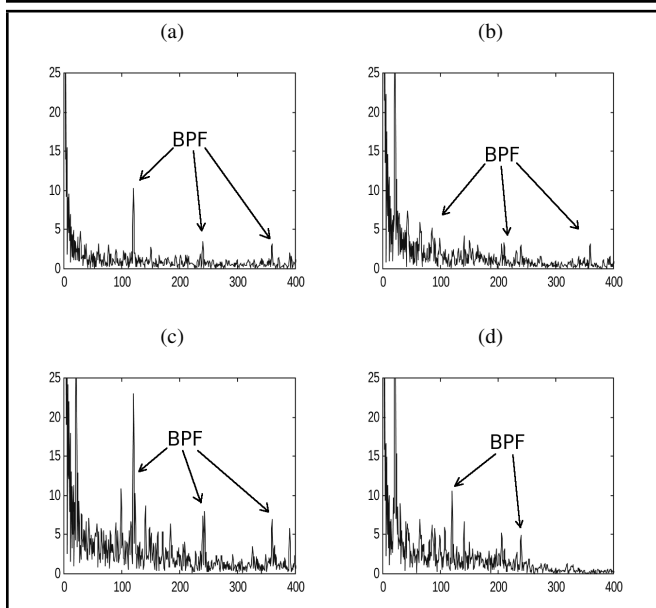


Figure 12: Envelope spectra demodulated from frequency band indicated (a) 6kHz – 24kHz, (b) 5kHz – 24kHz, (c) 4kHz – 24kHz, (d) 5kHz – 5.5kHz.

so it is hoped that the updated simulation model will help to explain the reason, mentioned in the introduction as a potential benefit of simulation.

5. INTERNAL COMBUSTION ENGINES

Powerful dynamic simulation packages such as LMS's Virtual Lab[®] and AmesSim[®] as well as ADAMS[®] have recently become available, with templates for a number of special situations, such as internal combustion (IC) engines. A typical diesel or spark-ignition engine can be modeled in terms of the dynamic properties of the rotating and reciprocating components, and structural dynamic properties of stationary components, such as the engine block and head. This gives the possibility of simulating a range of different faults, such as combustion faults, which affect the pressure time history in a given cylinder, and mechanical faults, such as piston slap, which can be simulated by increasing the clearance between piston and cylinder.

A very simple but powerful indicator of non-uniform combustion is given by the instantaneous angular velocity of the crankshaft, which can be obtained by frequency demodulation of a shaft-encoder signal from the crankshaft.²¹ The latter can be as simple as the series of pulses from a proximity probe detecting the passage of teeth on the ring gear.

Figure 13 gives a comparison of the instantaneous speed for a complete misfire in one cylinder of a 6-cylinder spark-ignition engine for a measured and a simulated case. A partial misfire in one cylinder gives a somewhat less obvious change in the speed but can be very well simulated. The technique used to obtain the measured result in Fig. 13(a) involved first a phase demodulation of the shaft-encoder signal, followed by differentiation to obtain the frequency modulation (i.e., angular velocity variation) signal. The latter was done by a $j\omega$ operation in the frequency domain, since it can then be combined with bandpass filtration to avoid enhancement of high-frequency noise and to remove low-frequency speed variations (at less than engine cycle frequency), which are unrelated to

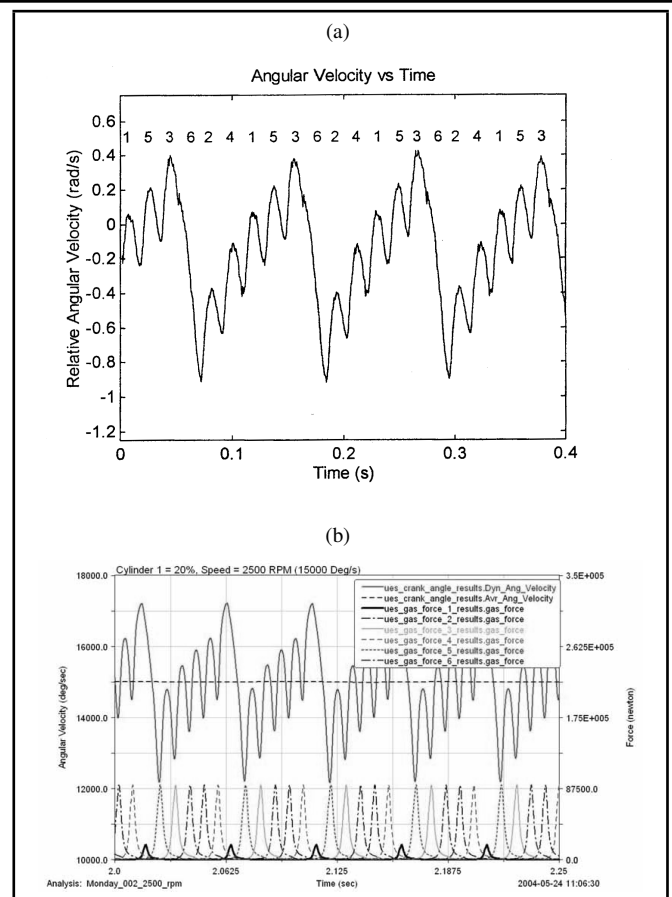


Figure 13: Angular velocity of the crankshaft for a misfire in one cylinder: (a) measured signal, (b) simulated signal.

engine condition. However, to obtain a fixed number of samples per cycle (for example, to train an ANN to recognize the pattern) it would be necessary to resample the signal using order analysis. An alternative way to obtain the instantaneous angular velocity very simply is to measure the time intervals between encoder pulses, using a very high-frequency clock (eg 20–80 MHz), and then invert the passage times and convert the result to crankshaft speed. This automatically gives a fixed number of samples per cycle. Such clocks are now available in commercial instrument systems.

The above discussion virtually assumes that the crankshaft is rigid, as a torque pulse applied from any cylinder gives a uniform response in terms of angular velocity. A somewhat larger engine with 20 cylinders has recently been simulated, where there are torsional vibration modes of the crankshaft excited by components within the running range of the engine. A paper on this work is being presented at the CM-MFPT conference in Dublin in June 2009.²² This demonstrates how a minimal amount of measurement information can be used to update a torsional vibration model of the crankshaft for the normal, healthy condition. Figure 14 is a schematic of the torsional model, where the generator is taken as running at fixed speed and therefore built-in for analysis purposes. It was in any case isolated by a flexible coupling tuned to about 9 Hz from the crankshaft. The inertias were reasonably well-known (using a standard formula to represent reciprocating components as equivalent rotating inertias), but stiffnesses less so. A genetic algorithm (GA) was used to optimise the values of the stiffnesses to match the first five natural frequencies, re-

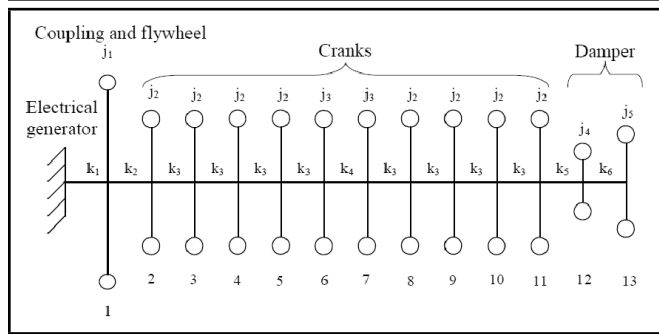


Figure 14: Torsional vibration model of crankshaft.

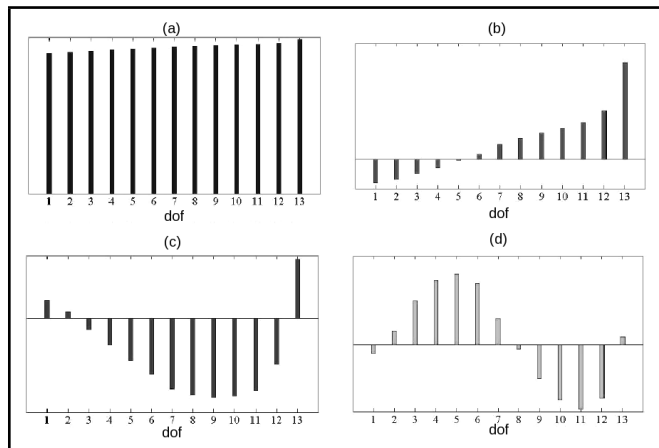


Figure 15: Estimated mode shapes: (a-d) represent modes 1-4, respectively.

sulting in the (unscaled) mode shapes (the first four) shown in Fig. 15. The x-axis (dof) represents the “degree-of-freedom” corresponding to each of the inertias (j_i) in the lumped parameter model.

Mode 1 is the almost-rigid body mode of the crankshaft on the coupling. Mode 2 is the damper mode, including some participation of the crankshaft as a spring. Modes 3 and 4 are the first two torsional modes of the crankshaft, and can be seen to approximate a 1/4 and 3/4 wavelength shape as modified by the damper. The estimated natural frequencies are compared with the measured ones (from a run-up in speed) in Table 1.

Measurements of torsional vibration were made with a torsional laser vibrometer (Polytec OFV-400) at the free end of the crankshaft on one side of the damper (dof 12).

Torque inputs from each cylinder were estimated on the basis of an estimated pressure curve for the load at the time of measurement. Since the aim of the modeling was to detect changes in condition, combustion abnormalities in particular, a parametric model of the pressure curve was made based on thermodynamic principles and the rate of heat re-

Table 1: Estimated and observed torsional resonance frequencies.

Mode	Estimated frequency (Hz)	Observed frequency (Hz)
1	7.2	9.4
2	33.2	37.3
3	63.0	51.8
4	132.4	≈ 125
5	210.2	≈ 200

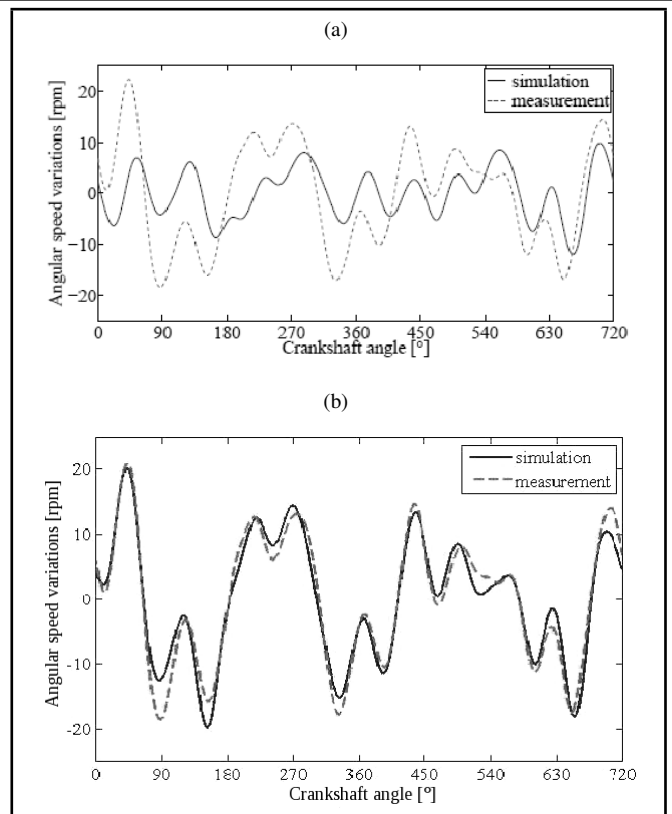


Figure 16: Simulated vs. measured responses: (a) initial estimates using analytical model, (b) final estimates using measured frequencies and optimised damping values.

leased (RoHR) corresponding to the fuel injection. A pressure trace was available for 75% load, and this was also fitted for the parameters using optimisation (GA followed by Levenberg-Marquardt least squares optimization), giving a very close match.

Torsional vibration responses at the measurement location were then made using the optimized model parameters, initially giving the result shown in Fig. 16(a). The result was greatly improved using the measured rather than the optimized analytical natural frequencies (but analytical mode shapes) and then by optimizing the damping values associated with each mode (originally taken from the 3 dB bandwidths of the peaks in the run-up curves).

As reported in Reference,²² it has been found possible to use this model to train ANNs to recognise departures from the normal condition, to localise the faulty cylinder, and to determine approximately the change in RoHR corresponding to the induced injector faults. The model was trained using two measurements of healthy condition spaced two years apart (and using the difference for an estimate of the standard deviation) and three measurements of induced injection faults on different cylinders made at the same time as the measurements of healthy condition. Details are in Reference.²²

6. CONCLUSION

Simulation of faults in machines may very well provide the only way of obtaining a sufficient number of signals to train artificial neural networks to detect and classify the potentially very wide range of faults that may be encountered. This paper demonstrates how such simulation can be done for bearings,

gears and their combination, as well as for internal combustion engines. The level of sophistication of the models ranges from relatively simple models, which can be used fairly generally to determine whether a particular fault condition exists, but not the severity of the condition; to powerful, detailed simulations of individual critical machines. The simulated signals can also be used to develop and test diagnostic methods and to study anomalous cases. Such examples are given for gears (to aid in distinguishing between tooth-root cracks and spalls) and bearings (to help explain an anomaly encountered).

7. ACKNOWLEDGMENTS

Results presented in this paper were provided by Yujin Gao, Dominique Ho, Hiroaki Endo, Nader Sawalhi, Mathieu Desbazeille and Peter Matthison, with much assistance from Jérôme Antoni. Much of the research on which it is based is supported by the Australian Government's DSTO through their Centre of Expertise in Helicopter Structures and Diagnostics at UNSW.

REFERENCES

- ¹ Bachschmid N., Pennacchi P. and Vania A. Thermally Induced Vibrations due to Rub in Real Rotors, *Journal of Sound and Vibration*, **299**(4–5), 683–719, (2007).
- ² Pennacchi, P. Computational Model for Calculating the Dynamical Behaviour of Generators Caused by Unbalanced Magnetic Pull and Experimental Validation, *Journal of Sound and Vibration* **312**, 332–353, (2008).
- ³ McFadden P. D. and Smith, J. D. Model for the vibration produced by a single point defect in a rolling element bearing, *J. Sound Vib.*, **96**(1), 69–82, (1984).
- ⁴ Ho, D. and Randall, R. B. Optimisation of bearing diagnostic techniques using simulated and actual bearing fault signals, *Mech. Systems and Signal Processing*, **14**(5), September, 763–788, (2000).
- ⁵ Randall, R. B. Training Neural Networks for Bearing Diagnostics using Simulated Feature Vectors". AI-MECH Symposium, Gliwice, Poland, 14–16 November, (2001).
- ⁶ Sawalhi N., and Randall, R. B. Semi-automated Bearing Diagnostics — Three Case Studies, Comadem conference, Faro, Portugal, June, (2007).
- ⁷ Feng, N., Hahn, E. J. and Randall R. B. Using transient analysis software to simulate vibration signals due to rolling element bearing defects, ACAM Conference, Sydney, February, (2002).
- ⁸ Fukata, S., Gad, E. H., Kondou, T., Ayabe T. and Tamura, H. On the Vibration of Ball Bearings, *Bulletin of JSME*, **28**(239), 899–904, (1985).
- ⁹ El Badaoui, M., Cahouet, Guillet, F., Daniere J., and Velex, P. Modelling and Detection of Localized Tooth Defects in Geared Systems, *Trans. ASME*, **123**, September, 422–430, (2001).
- ¹⁰ Howard I. and Jia X. The dynamic modeling of a spur gear in mesh, including friction and a crack, *Mech. Systems and Signal Processing*, **15**(5), 831–853, (2001).
- ¹¹ Bartelmus, W. Mathematical modeling and computer simulations as an aid to gearbox diagnostics, *Mech. Systems and Signal Processing*, **15**(5), 855–871, (2001).
- ¹² Endo, H., Randall, R. B. and Gosselin, C. Differential Diagnosis of Spalls vs Cracks in the Gear Tooth Fillet Region, *J. Failure Analysis and Prevention*, **4**(5), 57–65, (2009).
- ¹³ Endo, H. A study of gear faults by simulation, and the development of differential diagnostic techniques, PhD dissertation, UNSW, (2005).
- ¹⁴ Endo, H., Randall, R. B. and Gosselin, C. Differential diagnosis of spall vs. cracks in the gear tooth fillet region: Experimental validation, *Mech. Systems and Signal Processing*, **23**(3), 636–651, (2004).
- ¹⁵ Mark, W. D. and Reagor, C. P. Static-transmission-error vibratory-excitation contributions from plastically deformed gear teeth caused by tooth bending-fatigue damage, *Mech. Systems and Signal Processing*, **21**(2), 885–905, (2007).
- ¹⁶ Sawalhi N., and Randall, R. B. Simulating gear and bearing interactions in the presence of faults: Part I. The combined gear bearing dynamic model and the simulation of localised bearing faults, *Mech. Systems and Signal Processing*, **22**(8), 1924–1951, (2009).
- ¹⁷ Sawalhi N. and Randall, R. B. Simulating gear and bearing interactions in the presence of faults: Part II: Simulation of the vibrations produced by extended bearing faults, *Mech. Systems and Signal Processing*, **22**(8), 1952–1966, (2009).
- ¹⁸ Antoni, J. and Randall R. B., Differential Diagnosis of Gear and Bearing Faults, *ASME Journal of Vibration and Acoustics*, **124**, April, 165–171, (2002).
- ¹⁹ Sawalhi N. and Randall, R. B. A combined lumped parameter and finite element model of a single stage gearbox for bearing fault simulation, Comadem conference, Prague, June, (2008).
- ²⁰ Ho, D. and Randall, R. B. Manifestations of Bearing Fault Vibrations in Helicopter Gearboxes, Vertiflite Conference, Australian Defence Force Academy, Canberra, (1998).
- ²¹ Randall, R. B. Diagnostics of IC Engines from Torsional Vibration Measurements, CMVA Annual Conference, Edmonton, Canada, August, (2001).
- ²² Desbazeille, M., Randall, R. B., Guillet, F., El Badaoui, M. and Hoisnard, C. Fault detection and localization of a large diesel engine by analysing the instantaneous crankshaft angular speed, CM-MFPT conference, Dublin, 23–25 June, (2009).